5418
January 1991
(E)

STUDIES OF THE INTERACTIONS OF ELECTROWEAK GAUGE BOSONS*

D. L. Burke

Stanford Linear Accelerator Center
Stanford University, Stanford, California 94309

Presented at the 18th Annual SLAC Summer Institute on Particle Physics,
Stanford, CA, July 11-27, 1990.

* Work supported by Department of Energy contract DE-AC03-76SF00515.

Studies of the Interactions of Electroweak Gauge Bosons

Exploration of the electroweak interactions of quarks and leptons has ascended along the energy frontier for the past two decades, and has recently culminated in the elegant results obtained[1] with the SLC and LEP electron-positron colliders operating at the Z^0. The SU(2) isospin symmetry of the fermion sector is nearly completely known. It remains to uncover the top quark, and determine the precise relationship between the electroweak eigenstates and those of the mass operator embodied in the Cabibbo-Kobayashi-Maskawa formalism.

While our parameterization of the fermion sector of nature is becoming increasingly clear, we have no empirical knowledge of the interactions and possible structures of gauge bosons (with the exception, of course, of the massless photon). In this series of lectures we will review the origins of the interactions between gauge bosons that exist within the Standard Model, and explore signatures of new physics that might appear in the gauge-boson sector. Special attention will be given to pair-production of gauge bosons in e^+e^- annihilation at center-of-mass energies above those available at LEP II, and to scattering processes that could possibly be studied at very high energy e^+e^- and hadron colliders in the next century.

Origin of Gauge Boson Interactions in the Standard Model[2]

To formulate a Lagrangian that is invariant under local phase (gauge) transformations,

$$\psi(x) \rightarrow \psi'(x) = e^{i\alpha(x)}\psi(x), \tag{1}$$

we must be able to construct a suitable phase-covariant derivative with the property,

$$D_\mu\psi(x) \rightarrow e^{i\alpha(x)}D_\mu\psi(x). \tag{2}$$

As an example, we first consider the familiar construction of electromagnetism - an Abelian theory. In this case, Eq.(1) describes the transformation of fields with a U(1) symmetry. The observation that,

$$\delta_\mu(e^{i\alpha(x)}\psi(x)) = e^{i\alpha(x)}(\delta_\mu\psi(x) + i\psi(x)\delta_\mu\alpha(x)),$$

leads to the introduction of the vector gauge field,

$$A_\mu = (V, \vec{A}),$$

required to have the transformation property,

$$A_\mu \rightarrow A_\mu - \frac{1}{e}\delta_\mu(x)\alpha(x).$$

The needed covariant derivative and Lagrangian that successfully describe electromagnetic interactions of fermions are of the form,

$$D_\mu = \delta_\mu + ieA_\mu$$

and

$$\begin{aligned} L_{fermion} &= \bar{\psi}(i\gamma^\mu D_\mu - m)\psi \\ &= \bar{\psi}(i\gamma^\mu\delta_\mu - m)\psi - e(\bar{\psi}\gamma^\mu\psi)A_\mu. \end{aligned} \tag{3}$$

The kinetic energy of the fermion field is described by the first term in Eq.(3), while its electromagnetic current is seen to be just $\bar{\psi}\gamma^\mu\psi$.

To account for the energy and momentum carried by the gauge field itself, we note the covariant form of the field-strength tensor,

$$\begin{aligned} F_{\mu\nu} &= \frac{1}{ie}[D_\nu, D_\mu] \\ &= \delta_\nu A_\mu - \delta_\mu A_\nu + ie[A_\nu, A_\mu]. \end{aligned} \tag{4}$$

The last term in Eq.(4) vanishes for this Abelian case, so the gauge-invariant Lagrangian,

$$L_{gauge} \equiv -\frac{1}{4}F_{\mu\nu}F^{\mu\nu}$$

contains kinetic energies, but no terms trilinear in the photon field that would result in a photon-photon tree-level interaction.

It will be useful later to exhibit $F^{\mu\nu}$,

$$F^{\mu\nu} = \begin{pmatrix} 0 & E_1 & E_2 & E_3 \\ -E_1 & 0 & B_3 & -B_2 \\ -E_2 & -B_3 & 0 & B_1 \\ -E_3 & B_2 & -B_1 & 0 \end{pmatrix} \tag{5}$$

and to note the form of Maxwell's equations,

$$\begin{aligned} \delta_\mu F^{\mu\nu} &= -(\rho, \vec{J}) \\ \delta_\mu \tilde{F}^{\mu\nu} &= 0, \end{aligned}$$

where the dual field-strength tensor,

$$\tilde{F}^{\mu\nu} \equiv \frac{1}{2}\epsilon^{\mu\nu\alpha\beta}F_{\alpha\beta}$$

can be obtained from $F^{\mu\nu}$ by the interchange,

$$\begin{aligned} \vec{E} &\to \vec{B} \\ \vec{B} &\to -\vec{E}. \end{aligned}$$

An exact SU(2) symmetry leads to a more complex set of interactions among gauge bosons. Each of the generators of the symmetry,

$$\vec{\tau} = (\tau_1, \tau_2, \tau_3),$$

(e.g. Pauli matrices in a particular representation) must be properly gauged. We demand invariance of the Langrangian under phase transformations in isospin space,

$$\psi(x) \to e^{\frac{1}{2}\vec{\tau}\cdot\vec{\alpha}(x)}\psi(x)$$

and construct the covariant derivative,

$$D_\mu = I\delta_\mu + igB_\mu,$$

where D_μ, I, and

$$\begin{aligned} B_\mu &\equiv \frac{1}{2}\vec{\tau}\cdot\vec{b}_\mu \\ &= \frac{1}{2}\begin{pmatrix} b_\mu^3 & b_\mu^1 - ib_\mu^2 \\ b_\mu^1 + ib_\mu^2 & -b_\mu^3 \end{pmatrix}, \end{aligned}$$

are operators (e.g. 2×2 matrices).

The Lagrangian for the fermion matter fields becomes,

$$L_{fermion} = i\bar{\psi}(\gamma^\mu\delta_\mu - m)\psi - \frac{g}{2}\vec{b}_\mu\cdot\bar{\psi}\gamma^\mu\vec{\tau}\psi,$$

and a Lagrangian for the gauge fields can again be constructed from field-strength tensors (*c.f.* Eq.(4)),

$$\begin{aligned} F_{\mu\nu} &\equiv \frac{1}{2}\vec{F}_{\mu\nu}\cdot\vec{\tau} \\ &= \frac{1}{ig}[D_\nu, D_\mu] \\ &= \delta_\nu B_\mu - \delta_\mu B_\nu + ig[B_\nu, B_\mu]. \end{aligned}$$

The last term is not zero — rotations in three dimensions do not commute. Explicitly the field-strength tensor associated with generator l is of the form,

$$F_{\mu\nu}^l = \delta_\nu b_\mu^l - \delta_\mu b_\nu^l + g\epsilon_{jkl}b_\mu^j b_\nu^k. \tag{6}$$

The Lagrangian,

$$L_{gauge} = -\frac{1}{4}F_{\mu\nu}^l F^{l\mu\nu}$$

contains terms trilinear and quadrilinear in the fields that generate interactions at tree-level.

The broken $SU(2)_L \times U(1)_Y$ symmetry realized in nature requires the introduction of gauge fields that are mixed by the Higgs mechanism to yield the usual

physical states,

$$\begin{aligned} W^{\pm} &= b_1 \mp i b_2 \\ Z^0 &= -A\ sin\theta_W + b_3\ cos\theta_W \\ A^0 &= A\ cos\theta_W + b_3\ sin\theta_W. \end{aligned}$$

The Lagrangian can be written with these as,

$$L_{WWV}/g_{WWV} = i(W^{\dagger}_{\mu\nu}W^{\mu}V^{\nu} - W^{\dagger}_{\mu}V_{\nu}W^{\mu\nu}) + iW^{\dagger}_{\mu}W_{\nu}V^{\mu\nu}, \qquad (7)$$

where,

$$\begin{aligned} V^{\mu} &= A^0 \quad or \quad Z^0 \\ W^{\mu} &= W^{\pm} \\ W_{\mu\nu} &= \delta_{\mu}W_{\nu} - \delta_{\nu}W_{\mu}, \end{aligned}$$

and g_{WWV} is an overall normalization. These vertices all preserve C, P, and CP.

Notice first that the piece of $F^{l}_{\mu\nu}$ that is bilinear in the gauge field is antisymmetric in the generator indices (*i.e.* ϵ_{jkl}), and guarantees that $j \neq k \neq l$. The vertices,

$$Z^0Z^0Z^0$$
$$Z^0Z^0\ \gamma$$
$$Z^0\ \gamma\ \gamma$$

are all absent.

It is also instructive to consider a particular example. Take V to be a photon, so that $V_{\mu\nu} = F_{\mu\nu}$ as given in Eq.(5). Then, for example, the last term in the above Lagrangian contains a piece,

$$W^{\dagger}_{\mu}W_{\nu}F^{\mu\nu} \rightarrow (\epsilon^{ijk}W^{\dagger}_{i}W_{j})B^{k}.$$

We can identify this as a magnetic dipole interaction with magnetic moment $\mu^k = \epsilon^{ijk}W^{\dagger}_{i}W_{j}$. The Standard Model Lagrangian, in fact, contains only the lowest-order even-parity multipole interactions,

- Electroweak monopole ,
- "Magnetic" dipole ,
- "Electric" quadrupole.

The multipole moments of the charged boson states can be defined with respect to both neutral states — *i.e.* μ^{γ} and μ^{Z^0} can separately be defined and measured. We also note that, to this point, we have not considered interactions generated by the Higgs sector of the theory. We take this up in a later section of these lectures.

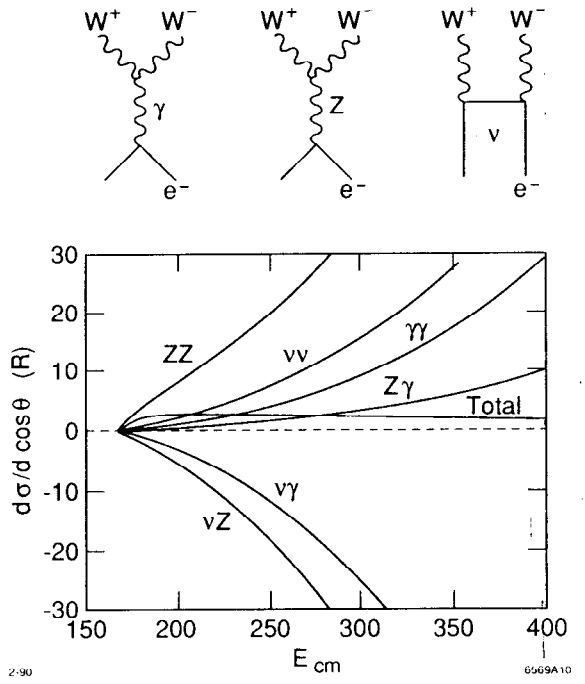

Figure 1. Form of the differential cross section (at $\cos\theta = 0$) for $e^+e^- \rightarrow W^+W^-$ as predicted by the Standard Model.

W-Pair Production in e^+e^- Annihilation

The production of pairs of gauge bosons near threshold has been well described in the literature[3] in preparation for physics studies at LEP II in the mid-1990's. Our discussion here will focus on the importance of obtaining detailed knowledge of the behaviour of this process at center-of-mass energies well above threshold. The Feynman diagrams of interest are shown in Fig. 1. The s-channel diagrams contribute only to the J = 1 partial wave, while all partial waves (except J = 0) are populated by the t-channel neutrino exchange. The Higgs propagator will produce an s-wave amplitude that is significant at very high energies, but the coupling to the electron is too weak to be of importance at foreseeable machines.

The $\Lambda = 2$ channel produced by neutrino exchange consists entirely of transversely polarized bosons, is well-behaved, and uninteresting. The $\Lambda = 1$ channel can produce $W_L W_T$ and $W_L W_L$ combinations, and is more exciting. The amplitudes for the three diagrams can be written[4]

$$\begin{aligned} \mathcal{M}^{\gamma}_{\lambda\bar{\lambda}} &= -A^{\gamma}_{\lambda\bar{\lambda}}\ \delta_{|\Delta|,1} \\ \mathcal{M}^{Z^0}_{\lambda\bar{\lambda}} &= A^{Z^0}_{\lambda\bar{\lambda}}\ [\delta_{|\Delta|,1} - \frac{1}{2sin^2\theta_W}\delta_{\Delta,-1}]\ \frac{s}{s-m_Z^2} \\ \mathcal{M}^{\nu}_{\lambda\bar{\lambda}} &= A^{\nu}_{\lambda\bar{\lambda}}\ [\frac{1}{2sin^2\theta_W}\ \delta_{\Delta,-1} - \frac{B_{\lambda\bar{\lambda}}\delta_{\Delta,-1}}{4sin^2\theta_W(1-cos\Theta)}] \end{aligned} \qquad (8)$$

where $\Delta \equiv \lambda_{e^-} - \lambda_{e^+}$ is the change in helicity of the fermion current, and $A_{\lambda\bar{\lambda}}$ and $B_{\lambda\bar{\lambda}}$ are functions of the center-of-mass energy, s. The helicity structure is particularly simple at $s >> m_Z^2$:

$(\lvert\lambda\rvert, \lvert\bar{\lambda}\rvert)$	$A^{\gamma} = A^Z = A^{\nu}$	B
(1,1)	1	γ^{-2}
(0,1)	2γ	γ^{-2}
(1,0)	2γ	γ^{-4}
(0,0)	$2\gamma^2$	γ^{-4}

where $\gamma = p_W/m_W$.

It is important that A^{γ}, A^Z, and A^{ν} become equal at high energies, since those parts of the cross section that correspond to the production of longitudinal bosons are not individually well-behaved. Unitarity is restored only through a delicate balance of the individual amplitudes that can be seen by setting the three coefficients equal in Eq.(8). This is graphically depicted in Fig. 1. A cross section calculated from any subset of the diagrams diverges rapidly — as s/m_W^2.

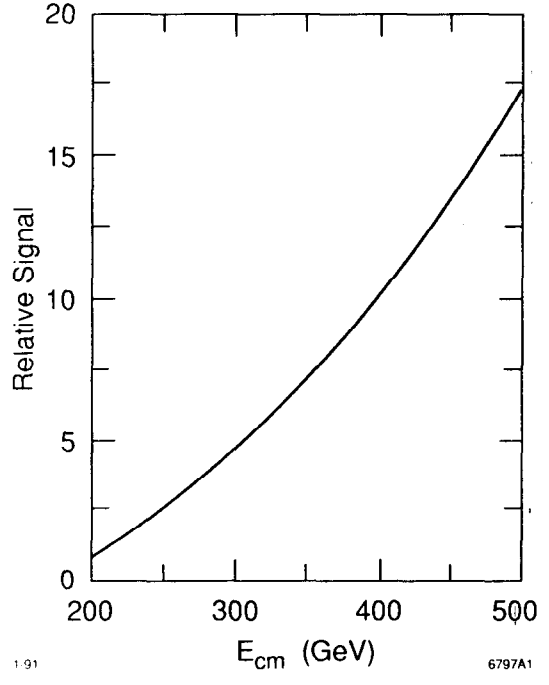

Figure 2. Growth of anomalies in the cross section for $e^+e^- \rightarrow W^+W^-$ as the center-of-mass energy is increased beyond threshold. The curve is given by $\beta^2 \cdot s/m_W^2$.

The source of these divergences is readily uncovered. Consider the form of the amplitude for producing a pair of longitudinally polarized states,

$$\begin{aligned}\mathcal{M}_{LL} &\sim \epsilon_\mu^L(k)\cdot\epsilon^{L\mu}(k) \\ &\sim (\frac{k}{m},0,0,\frac{k}{m})\cdot(\frac{k}{m},0,0,-\frac{k}{m}),\end{aligned} \tag{9}$$

where $\epsilon_\mu^L(k)$ are polarization vectors. The resulting cross section,

$$\frac{d\sigma^{LL}}{dcos\theta} \sim \frac{s}{m_W^2}\cdot sin^2\theta,$$

clearly exhibits the γ^2 behaviour indicated in the above table. Any anomaly in the couplings between gauge bosons will lead to effects in the longitudinal-pair cross section that can be expected to grow rapidly as the center-of-mass energy is increased above threshold. There is an additional enhancement due to the growth of phase space available for the production of longitudinally polarized states. Fig. 2 shows that the combined effect is quite dramatic — an increase in beam energy of a factor of two over LEP II energies leads to an order of magnitude increase in sensitivity to deviations from the Standard Model.

Production of $W^\pm$ pairs above threshold occurs with a cross section that is larger than any other single process. At $s \approx 500$ GeV this cross section, shown in Fig. 3, is twice the total QCD cross section, and grows asymptotically (in units of R) by another factor of two. Near threshold essentially all pairs are transversely polarized, and the cross section grows like β.

The helicity structure of the production and decay of W-pairs is extremely rich. Examples are shown in Fig. 4. The dominant forward peak is generated by the t-channel neutrino exchange, while in the backward direction, the s-channel production of longitudinal states becomes appreciable. This changing polarization of the boson state can be observed by analysis of its leptonic decay. The decay angle, denoted by χ and defined as the angle between the charged lepton and the initial boson flight direction boosted to the W rest frame, is shown Fig. 4 for three different

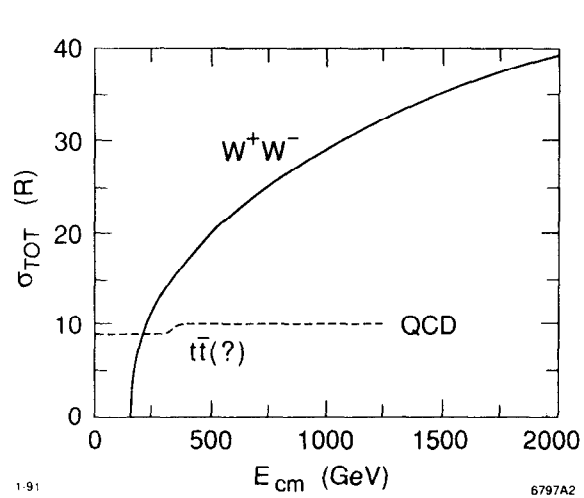

Figure 3. Cross sections (in units of R) for W-pair and QCD final states. The step in the QCD rate indicated for $t\bar{t}$ production is approximately one unit.

boson production angles. Notice that the three-momentum of the neutrino that is undetected can be completely reconstructed from constraints of energy-momentum conservation and the known W mass. This will be true even for events with significant initial-state radiation or beamstrahlung, since the system is overconstrained and even the missing radiation can be reconstructed.

Signatures of New Physics in W^+W^- Final States

Experimental studies of the reaction $e^+e^- \to W^+W^-$ carried out at center-of-mass energies $\sim$ 400-500 GeV will be optimally situated to look for substructure in the boson states or new physics in their interactions. The most general CP-conserving Lagrangian for this process can be written[5],

$$\begin{aligned}L_{WWV}/g_{WWV} = {} & ig_1^V(W_{\mu\nu}^\dagger W^\mu V^\nu - W_\mu^\dagger V_\nu W^{\mu\nu}) \\ & + i\kappa_V W_\mu^\dagger W_\nu V^{\mu\nu} + i\frac{\lambda_V}{m_W^2}W_{\lambda\mu}W_\nu^\mu V^{\nu\lambda} \\ & + g_5^V\epsilon^{\mu\nu\alpha\beta}(W_\mu^\dagger \overleftrightarrow{\delta}_\alpha W_\nu)V_\beta,\end{aligned} \tag{10}$$

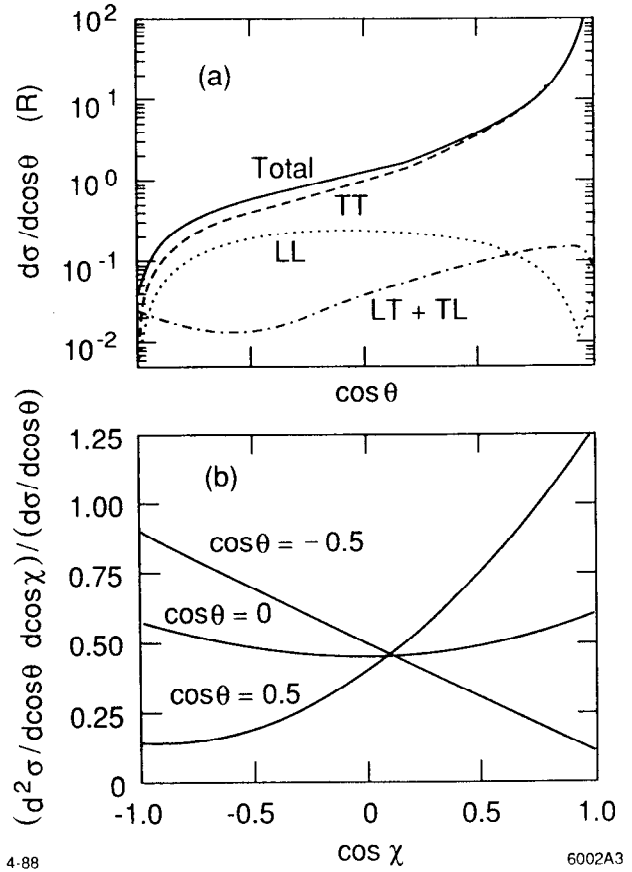

Figure 4. Angular distributions for the production and decay of W-pairs in e^+e^- annihilation. The decay distributions are given for three different production angles. The production angle is defined as the polar angle of the W^- measured with respect to the e^- beam direction.

where $A\overleftrightarrow{\delta}B = A(\delta B) - (\delta A)B$. The Standard Model result (Eq.(7)) is recovered with,

$$g_1^V = \kappa_V = 1$$
$$\lambda_V = g_5^V = 0.$$

We note that the g_5^V term violates both C and P, and will ignore it. It is most common to parameterize the sensitivities of various experimental opportunities in terms of κ_V and λ_V.

An example is again useful. For $V = \gamma$ we saw earlier that g_1^γ and κ_γ account for the electric charge, magnetic dipole, and electric quadrupole moments of the $W^\pm$. Consider a piece of the λ_γ term:

$$W_{\lambda\mu}W_\nu^\mu F^{\nu\lambda} \rightarrow \delta_\mu W_\lambda W_\nu^\mu F^{\nu\lambda}$$
$$= W_\lambda W_\nu^\mu \delta_\mu F^{\nu\lambda}.$$

The second line follows after one integration by parts. The $\lambda = 0$ terms are of the form,

$$(W_0 W^{ij})\delta_i E_j$$

which is just an electric quadrupole interaction. The general parity-conserving electroweak magnetic dipole and electric quadrupole moments of the W are given by,

$$\mu_W^V = \frac{e}{2m_W}(1 + \kappa_V + \lambda_V)$$
$$Q_W^V = -\frac{e}{4m_W^2}(\kappa_V - \lambda_V),$$

with conventional $(g-2)_W = (\kappa - 1) + \lambda$. Deviation of κ from unity or λ from zero would indicate new physics beyond the Standard Model.

Limits on the values of κ and λ have been set[6] from analyses of existing data. The ratio of neutral-current and charged-current neutrino interaction cross-sections depend upon boson loop corrections to the t-channel weak propagators. These corrections are sensitive to the strength of the three-boson vertex, but their evaluation requires the introduction of a cut-off for the loop integrals. The correlated limits on κ_Z and κ_γ are given in Fig. 5 for a cut-off parameter of 1 TeV. A corresponding set of limits for λ_Z and λ_γ have been set by analysis of the electroweak scale

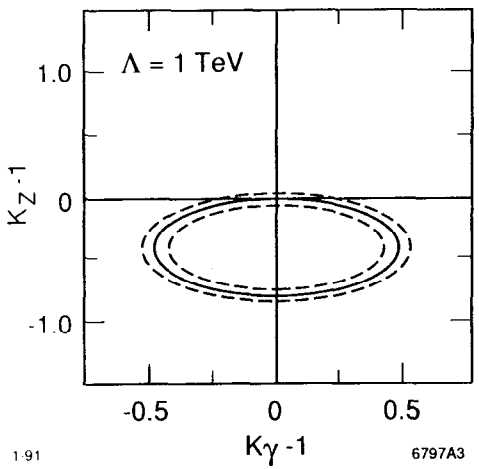

Figure 5. Limits on κ parameters deduced from existing data. See text for description.

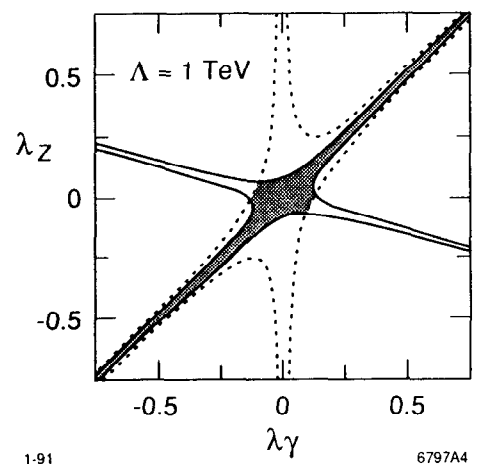

Figure 6. Limits on λ parameters deduced from existing data. See text for description.

parameters, G_F, α, $sin^2\theta_W$, and the mass of the Z^0. The s-channel weak propagators also depend upon loop corrections that require knowledge of the three-boson vertex. The limits shown in Fig. 6 are evaluated with a cut-off of 1 TeV in the loop integrals. Additional constraints on κ and λ can be inferred from the requirement that electroweak cross sections remain unitary at high energies. These are typically of order unity. Taken together, these limits are:

$$|\lambda_\gamma| \leq 0.6 \qquad |\kappa_\gamma - 1| \leq 1.0$$
$$|\lambda_Z| \leq 0.6 \qquad -0.8 \leq \kappa_Z - 1 \leq 0.$$

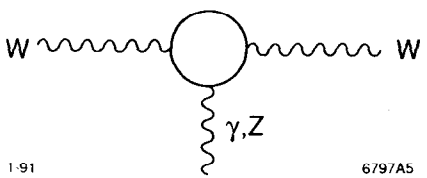

Figure 7. Loop corrections to boson propagators that generate anomalous moments.

There are loop corrections to the W and Z propagators that are expected in the Standard Model. These loops, shown in Fig. 7, generate apparent anomalous moments. The complete Standard Model correction depends (at the factor of two level) on the mass of the top quark and the Higgs sector[7], but at $q^2 \approx 0$, and $m_t \gg m_W$ and $m_H \gg m_W$,

$$(g-2)_W \approx 1.8 \frac{\alpha}{\pi} \sim 0.01.$$

This is clearly well below the sensitivity of present experimental data.

Experiments in the near future at Fermilab and LEP will provide additional

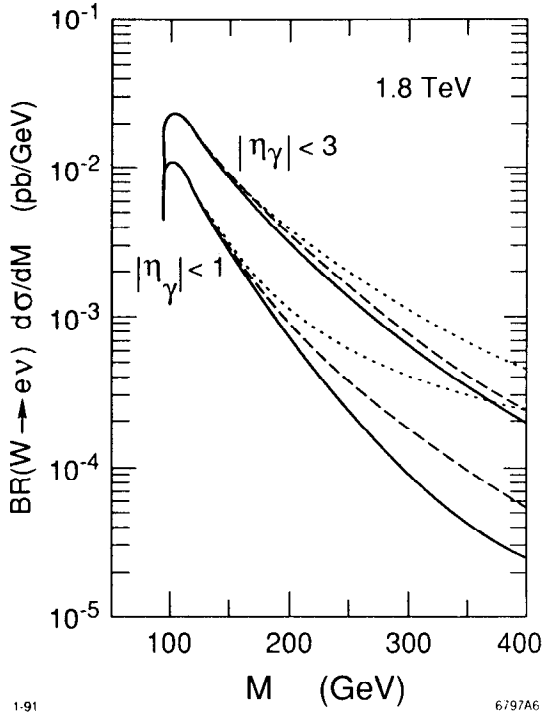

Figure 8. Differential cross section for production of $W\gamma$ events at the TEVATRON. The solid curves give the Standard Model expectation, the dots correspond to $\lambda_\gamma = 0.5$, and the dashed curves are for $\kappa_\gamma - 1 = 1.0$.

tests of boson couplings. The processes,

$$\begin{aligned} q\bar{q} &\rightarrow W^\pm\gamma \\ &\rightarrow W^\pm Z^0 \\ &\rightarrow W^+W^-, \end{aligned}$$

will be studied at the TEVATRON collider. (See lectures by S. Errede at this school.) The $W^\pm\gamma$ final state can be detected when the W decays leptonically. The cross section[8], shown in Fig. 8, depends upon κ_γ and λ_γ. It is estimated that after the CDF experiment accumulates a data sample of 100 pb^{-1}, the cross section can be measured well enough to be sensitive to,

$$\begin{aligned} |\lambda_\gamma| &\geq 0.4 \\ |\kappa_\gamma - 1| &\geq 1.0. \end{aligned}$$

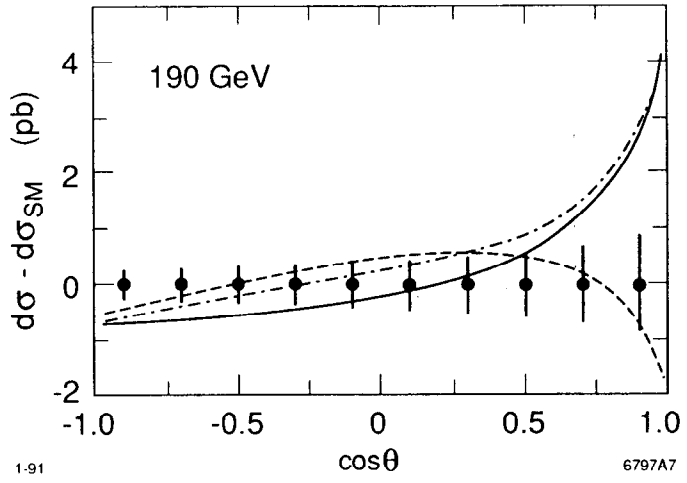

Figure 9. The expected accuracy of measurements to be made at LEPII with a data exposure of 500 pb^{-1} compared to signals generated by anomalous moments of the W. The solid curve corresponds to $\kappa_Z - 1 = 0.5$; the dashed curve to $g_5^Z = 0.5$, and the dot-dashed curve to $\lambda_Z = 0.5$.

Although limited because of its restricted energy range, LEP II will provide the greatest sensitivity to the structure of gauge boson interactions that will be available in the mid-1990's. Approximately 4000 W-pair events will be produced, with at least one of the bosons tagged by its decay to an electron or muon, if experiments are able to acquire integrated luminosities of 500 pb^{-1}. The statistical accuracy with which the differential cross section can be measured is compared[5] to several theoretical curves in Fig. 9. If κ_γ or λ_γ differ from their Standard Model values by more than $\sim$ 0.2, then it should become apparent in these experiments.

Future e^+e^- Colliders

Efforts are in progress at laboratories around the world to understand and develop the accelerator physics and technology necessary for the construction and operation of future electron-positron colliders. These machines will almost certainly be linear colliders. (See lectures by R. Ruth at this school.) One feature of a linear machine is that its center-of-mass energy can be increased over that of its original operating point by making improvements in the power sources so to generate higher accelerating fields, or by increasing the length of the accelerator, or both. Studies have shown that it is reasonable to expect a machine built with a given technology (*e.g.* *rf* frequency and alignment precision) to be expandable by about a factor of three in energy. It is difficult to optimize the luminosity of a particular machine over a much larger range of energy. Design efforts have concentrated on machines with center-of-mass energies that start at $\sim$ 0.5 TeV, and expand into the TeV region with luminosities of $10^{33} - 10^{34}\text{cm}^{-2}\text{s}^{-1}$. For lack of a better name, we call this the NLC — the *N*ext *L*inear *C*ollider.

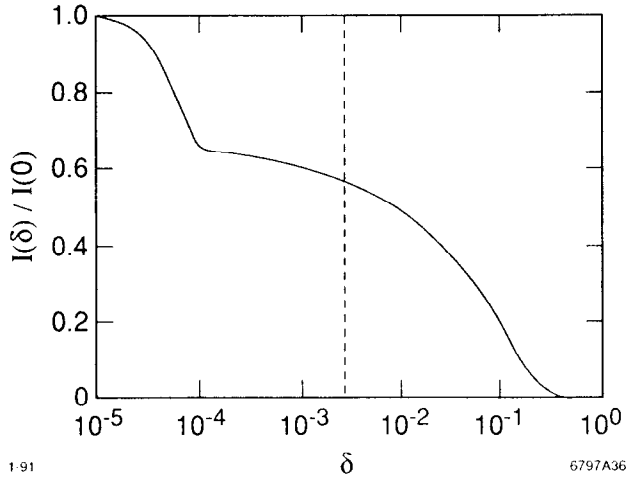

Figure 10. Beamstrahlung in a multi-bunch linear collider at 500 GeV center-of-mass energy. The parameter $\delta \equiv 1 - s^{\frac{1}{2}}_{collision}/2E_b$.

Coherent phenomena that occur during the beam-beam interaction will become important at future high-energy high-intensity colliders. One such process that is important to understand is "beamstrahlung" — the radiation emitted by beam particles as they pass through the coherent electromagnetic field of the opposing bunch[9]. Energy loss due to beamstrahlung is relatively small in multi-bunch machines operating at energies $E_{cm} \sim 500$ GeV (see Fig. 10), so energy-momentum constraints remain powerful tools for the analysis of data, just as they are at present-day facilities. Machines can be designed with stronger beam-beam interactions. These generally achieve higher total luminosity, but much of the gain is from collisions at lower center-of-mass energies. Since the annihilation cross section is larger at lower energies, the distribution of annihilation events in center-of-mass energy can be nearly flat, as shown in Fig. 11. Kinematic constraints are less useful in this situation, although it is still possible to impose transverse momentum conservation in the analysis of a number of final states to improve mass resolutions and reject

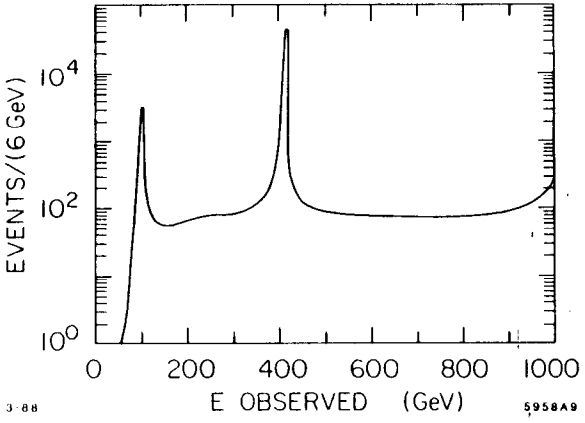

Figure 11. Spectrum of hadronic events produced by e^+e^- annihilation at a machine with nominal center-of-mass energy 1 TeV, but with a large beamstrahlung parameter ($\Upsilon = 1.6$). A peak due to radiation to the Z^0 is evident, and a hypothetical new Z' resonance has been included ($m_{Z'} = 400$ GeV) for illustrative purposes.

backgrounds.

The Physics Environment at the NLC

From 3 GeV to the Z^0 mass, e^+e^- collisions have been observed to give events with a simple and transparent structure. Annihilation events, that carry the full beam energy, dominate over peripheral reactions. Final states are usually two-jet-like and almost always highly planar. This feature makes searches for new, heavy particles straightforward, and minimizes biases and backgrounds to precision studies of strong and electroweak interactions. Recently, the power of the e^+e^- environment was emphasized in the performance of the Mark II experiment at the SLC[10]. With an event sample of ≈ 600 Z^0's, and using an upgrade of a detector originally built to study physics at SPEAR energies, the Mark II group reported limits on new heavy quarks and neutral leptons to within 90% of the kinematic limit for pair production, and measured the peak Z^0 cross section precisely enough to rule out (at 95% CL) the existence of a fourth generation of quarks and leptons with a massless neutrino. This remarkable cleanliness will also occur at TeV energies.

The Standard Model processes that will be predominant at the NLC (E_{cm} = 500 GeV) are:

Final State	Cross Section (R)	Events/(10fb^{-1})
QCD (*udscb*)	9	31,000
W^+W^-	20	70,000
Z^0Z^0	1.2	4,200
$t\bar{t}$ (m_t = 150 GeV)	1	3,500

It is common to use 10^7 seconds as the total running time for an accelerator in a calendar year — a so-called "Snowmass Year". In this time, a machine with luminosity 10^{33} cm^{-2} sec^{-1} will deliver 10 fb^{-1}.

Existing technology is sufficient to build detectors capable of fully exploiting the physics opportunities offered by high-energy e^+e^- linear colliders. Calorimetery becomes an increasingly important tool for accurate reconstruction of the parton four-vectors in each event as the center-of-mass energy is increased. Studies done to date[11] have used simulations of detectors with capabilities similar to those of SLC and LEP detectors:

Hadronic Calorimetery	$50\%/\sqrt{E} \oplus 2\%$
Electromagnetic Calorimetery	$8\%/\sqrt{E} \oplus 2\%$
Electron/Pion Energy Ratio	1.0 ± 0.1
Calorimeter Segmentation	4° towers
Charged Particle Tracking	$\sigma_p/p = 3 \times 10^{-4} p$

Precise reconstruction of the vertex of each event, and the impact parameters of each track, is important in order to fully explore the physics. Vertex detectors with impact-parameter resolutions given by,

$$\sigma_b^2 = (5\mu m)^2 + \left(\frac{50\mu m \cdot GeV}{p}\right)^2$$

exist today, and are sufficient to do the physics at the NLC.

The solid-angle coverage of NLC detectors will likely be compromised by the need to install machine components near the interaction region, and by the presence of low-angle machine-induced backgrounds. Studies have assumed that the detector is hermetic, except at regions within 10° of the beamline. It is generally assumed that no particles except low-angle Bhabha scatters will be detected at smaller polar angles.

Simple jet-finding algorithms quickly and accurately reproduce the underlying parton structure of each event with little bias from uncertainties in fragmentation processes and little ambiguity from the overlap of decay products from differing parton showers. A typical event is shown in Fig. 12 as it would be observed in the tracking chamber of a detector with a 1 Tesla solenoidal field. We show in Fig. 13 the masses in opposite thrust hemispheres of standard model e^+e^- annihilation events as they would be reconstructed by a detector with the above parameters. Only

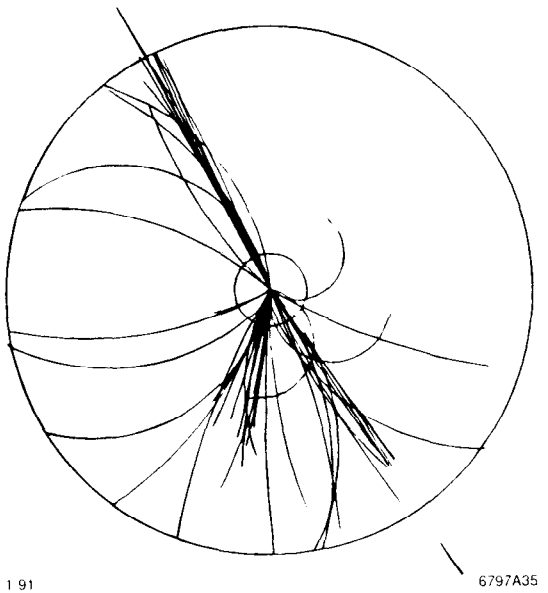

Figure 12. Annihilation event of the type $e^+e^- \to b\bar{b}g$ as observed at $E_{cm} = 1$ TeV.

simple cuts on total energy and thrust direction were made to select events for this figure. The peak at the W mass stands out clearly above the background from $q\bar{q}$ production, as do the single-prong leptonic decays. Gauge bosons are easily identified, and each event can be accurately reconstructed.

Studies of Gauge Boson Interactions at the NLC

W-Pair Production. As discussed earlier, we can expect significant gains in sensitivity to new physics in careful studies of the reaction,

$$e^+e^- \to W^+W^-$$

as the center-of-mass energy is increased above production threshold. What can be achieved with a full helicity analysis of this process is presently under investigation[12], but initial results demonstrate the point clearly. Shown in Fig. 14 are the dependencies on the parameters κ_γ and λ_γ of the total W-pair cross section and the forward-backward asymmetry,

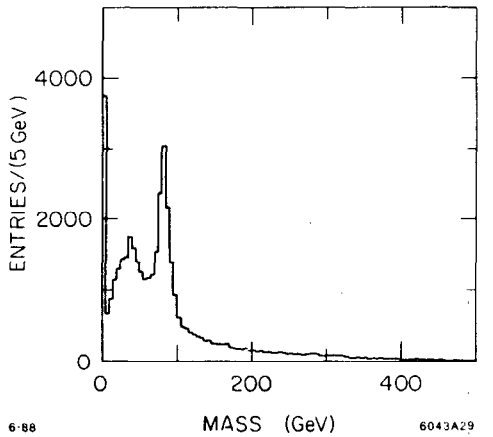

Figure 13. Reconstructed invariant masses in the forward and backward thrust hemispheres of standard model processes.

$$A_{FB} \equiv \frac{N^+ - N^-}{N^+ + N^-}.$$

The number N^+ is defined as the number of events with the W^- boson in the forward hemisphere ($cos\theta > 0$, with θ measured with respect to the incident e^- direction). A data exposure of 10 fb^{-1} will yield $\approx 10^4$ W-pair events tagged with one electron or muon leptonic decay, so measurement of the total cross section with 3% total error, and of the forward-backward asymmetry with error ≈ 0.01 can be achieved. Such results would be sensitive to values of κ_γ or λ_γ that differ from their Standard Model values by more than a few times 0.01 — an order of magnitude better than expected at 200 GeV.

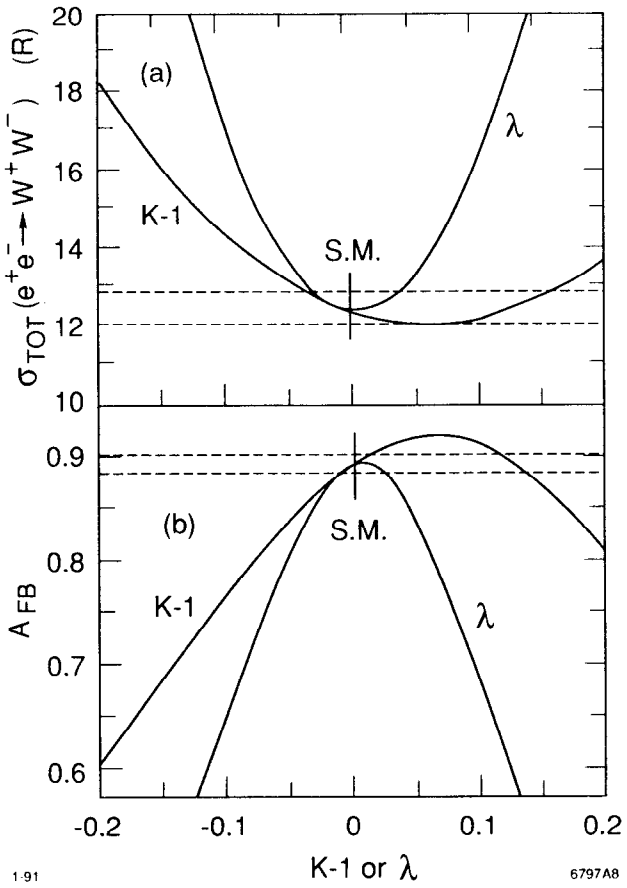

Figure 14. Dependence of W-pair cross sections on the values of κ and λ described in the text. The dashed lines indicate the estimated experimental accuracy with which the cross section and asymmetry can be measured.

Photon-W Scattering. The s-channel W-pair process proceeds by both photon and weak neutral propagators, and so will be modified by non-Standard values of any of the parameters κ_γ, λ_γ, κ_Z, or λ_Z. It is possible to isolate the photon couplings

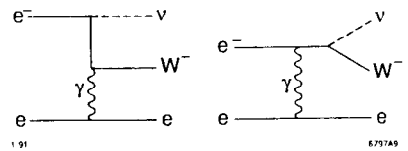

Figure 15. Feynman graphs that contribute to the $e\nu W$ final state.

in a different combination in the process,

$$e^+e^- \to e\nu W$$

that receives contributions from the graphs shown in Fig. 15. The signature of this process is the presence of a single electron or muon from the decay of the boson in the final state. The scattered beam electron (or positron) typically remains at very small polar angles, and goes undetected. The measured cross section can be normalized by detection of the Compton process,

$$e\gamma \to e\gamma,$$

in which case, uncertainties in the equivalent photon flux are eliminated.

The variation of the cross section with non-Standard values of κ_γ and λ_γ is shown in Fig. 16. A 3% measurement of the rate yields good sensitivity to differing values of κ_γ. A summary of the limits[13] from this process and the W-pair forward-backward asymmetry is given in Fig. 17. The estimated[14] sensitivity of experiments at the SSC is also shown in the figure. The Standard Model predicts values that depend on the unknown masses of the top quark and Higgs boson, but are within the shaded area shown on the plot.

Further studies of the spin structure of gauge-boson production at electron-positron colliders are necessary to determine if it will be possible to probe to the level of the expected Standard Model corrections[12], but it is apparent that a 500 GeV e^+e^- collider provides greater sensitivity to new physics than will be attainable at much higher energy hadron colliders.

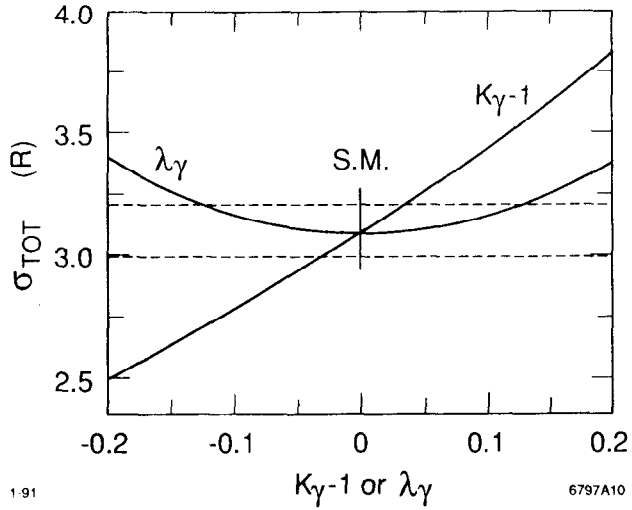

Figure 16. Dependence of the cross section for the $e\nu W$ final state on values of κ and λ. The dashed lines indicate the accuracy with which the cross section can be measured.

A Composite Model

Composite models generally predict large deviations from the Standard Model expectations for the interactions of gauge bosons. As an example, we consider a model[15] that successfully reproduces the spectra and phenomenology of the Standard Model at mass scales below a few hundred GeV. Preons are confined in a manner patterned after QCD with a confining scale,

$$\Lambda \sim G_F^{-1} \approx 300\ GeV.$$

An underlying unbroken SU(2) symmetry guarantees the correct electroweak boson mass relations, and weak forces appear as "Van der Waals" remnants of the preon binding potential. This model is structured so that it violates no presently observed quantity, including light quark and lepton anamolous moments[16]. This is not the case for the heavier (and therefore less tightly bound) top quark, and W and Z boson

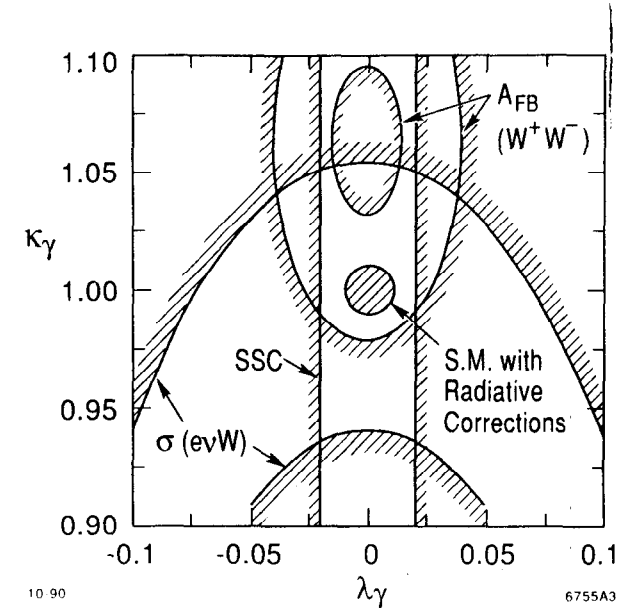

Figure 17. Limits on structure in gauge boson interactions attainable in e^+e^- annihilation and at the SSC. The values predicted by the Standard Model depend on the masses of the top quark and the Higgs boson, but lie somewhere in the shaded area.

states. Shown in Fig. 18 are the predicted values of κ and λ that are generated in this model by preons of various mass. The values are well within the sensitivity of the experiments that we have been discussing.

CP-Violation in Gauge Boson Interactions

We have so far constructed the WWV Lagrangian from CP-conserving interactions. In addition to the four terms in Eq.10, there are three possible CP-violating forms that satisfy Lorentz and gauge invariance,

$$\begin{aligned} L^{CP}_{WWV}/g_{WWV} &= -g_4^V W_\mu^\dagger W_\nu(\delta^\mu V^\nu + \delta^\nu V^\mu) \\ &+ i\tilde{\kappa}_V W_\mu^\dagger W_\nu \tilde{V}^{\mu\nu} + i\frac{\tilde{\lambda}_V}{m_W^2} W_{\lambda\mu} W_\nu^\mu \tilde{V}^{\nu\lambda}, \end{aligned} \tag{11}$$

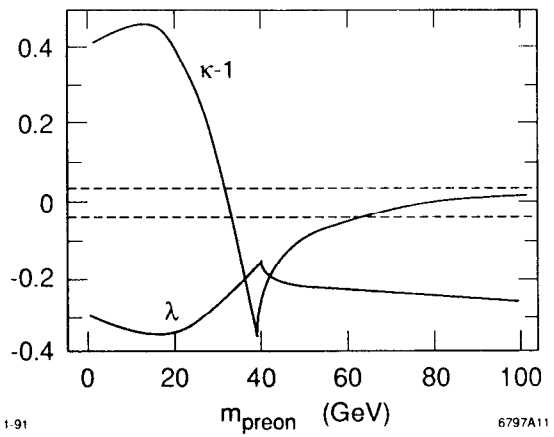

Figure 18. Values of κ and λ generated in a composite model by preons of various mass.

where $\tilde{V}^{\mu\nu} = \frac{1}{2}\epsilon^{\mu\nu\alpha\beta}V_{\alpha\beta}$ is the dual of $V_{\alpha\beta}$. Notice that, combined with the CP-conserving Lagrangian, this saturates all possible structure in the e^+e^-cross section. There are nine possible W^+W^- helicity states, but two with $J = \pm 2$ are not accessible through the annihilation channel.

Consider, as we have before, the particular case $V = \gamma$. The dual $\tilde{F}^{\mu\nu}$ is obtained from $F^{\mu\nu}$ by interchange of the electric and magnetic fields. Apparently, a non-zero value of either $\tilde{\kappa}_V$ or $\tilde{\lambda}_V$ introduce electric dipole and magnetic quadrupole moments,

$$d_W^V = \frac{e}{2m_W}(\tilde{\kappa}_V + \tilde{\lambda}_V)$$
$$\hat{Q}_W^V = -\frac{e}{m_W^2}(\tilde{\kappa}_V - \tilde{\lambda}_V).$$

These parity-violating interactions are identified in atomic physics as E1 and M2 transitions.

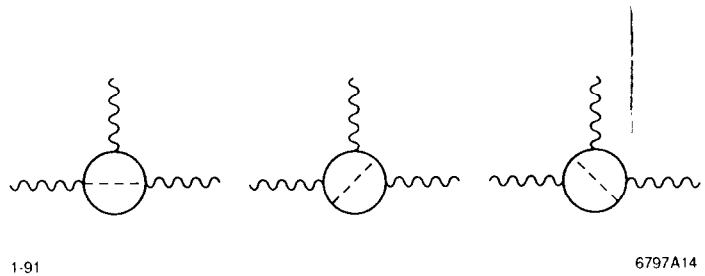

Figure 19. Two-loop corrections to the vector gauge boson propagator generated by Higgs particles.

Model-dependent constraints on $\tilde{\kappa}$ and $\tilde{\lambda}$ can be inferred from experimental limits on the electric dipole moment of the neutron[17],

$$d_n < 1.2 \times 10^{-25} e \cdot cm.$$

Generation of an electric dipole moment for the W-boson will occur through two-loop corrections to the propagator (Fig. 19). If there is but a single neutral Higgs particle, then these corrections will create little effect, but in models with more than one Higgs doublet, considerably larger moments can occur. A similar correction will occur to the gluon propagators that make up part of the neutron wave-function[18]. It is necessary to assume some model for the neutron wave function in order to relate the experimental limit on its dipole moment to the strength of the Higgs correction. To provide a framework, SU(6) has been used[19] to estimate that $\tilde{\lambda}_W$ will be of order 10^{-4} or less.

CP Violation in High Energy e^+e^-Interactions

The CP-violating Lagrangian (Eq.11) will generate imaginary pieces to the helicity amplitudes in the W-pair final state. The resulting interference between the various amplitudes will lead to directly observable correlations between the production and decay properties of the W-bosons. Leptonic decays of the produced bosons

can be analysed to yield the differential cross section[20],

$$\frac{d\sigma}{dcos\Theta dcos\theta dcos\phi} \sim sin\phi\left[Im(\Gamma_{+0})(1-cos\theta)+Im(\Gamma_{01})(1+cos\theta)\right]sin\theta/\sqrt{2}$$
$$+\ cos\phi\left[Re(\Gamma_{+0})(1-cos\theta)+Re(\Gamma_{01})(1+cos\theta)\right]sin\theta/\sqrt{2}$$
$$+\ sin2\phi Im(\Gamma_{-+})sin^2\theta/2\ +\ cos2\phi Re(\Gamma_{-+})sin^2\theta/2,$$

where Θ is the production angle of the W-boson, and θ and ϕ are the angles of the lepton momentum in the rest-frame of the W. The helicity amplitudes, $\Gamma(\Theta)$, are determined by the values of g_4, $\tilde{\kappa}_V$, and $\tilde{\lambda}_V$.

Theoretical calculations are needed to clarify the range of $\tilde{\kappa}$ and $\tilde{\lambda}$ that are of interest for various extrapolations of the Standard Model, and Monte Carlo studies are needed to determine the sensitivities of experiments to these effects.

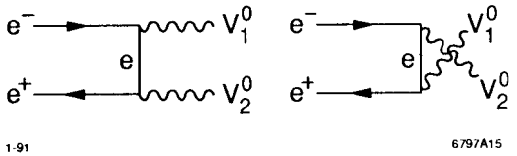

Figure 20. Feynman diagrams for the production of neutral gauge bosons in e^+e^- annihilation .

Neutral Gauge Boson Pairs

The tree-level Standard Model diagrams that lead to pairs of neutral gauge bosons in e^+e^- annihilation are shown in Fig. 20. The cross sections (Fig. 21) are peaked symmetrically in the forward and backward hemispheres[21]. The possible forms in the Lagrangian for the production of $V_1^0 = V_2^0 = \gamma$ or Z^0 are constrained by Bose symmetry, and there is no s-channel rate at the lowest order. These cases are not especially of interest, since the W-pair final state occurs with a considerably higher cross section, and it is not likely that new physics would occur in the neutral channels that does not also occur in the charged channel.

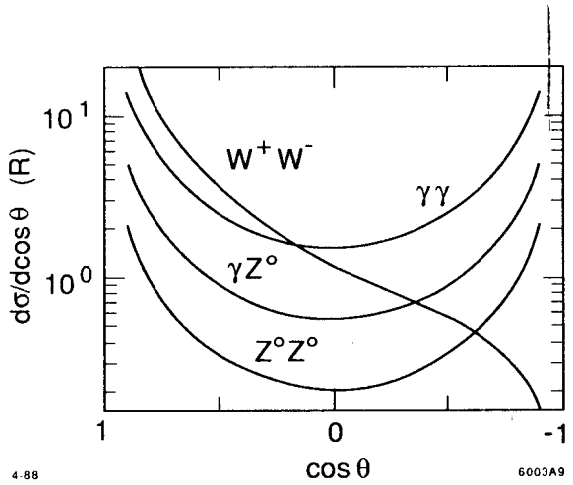

Figure 21. Differential cross sections for neutral gauge boson pairs produced by e^+e^- annihilation .

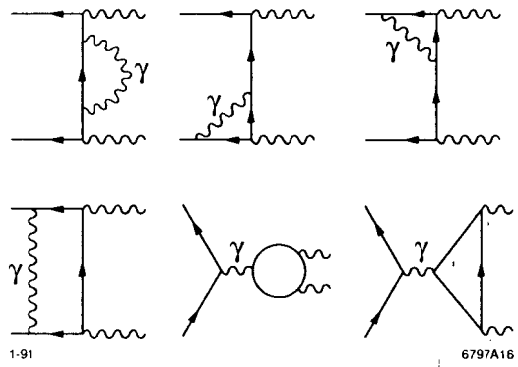

Figure 22. QED and weak neutral current loop corrections to the production of neutral gauge bosons in e^+e^- annihilation .

There is, however, a particular experimental reason[22] for looking more closely at the process,

$$e^+e^- \rightarrow \gamma Z^0.$$

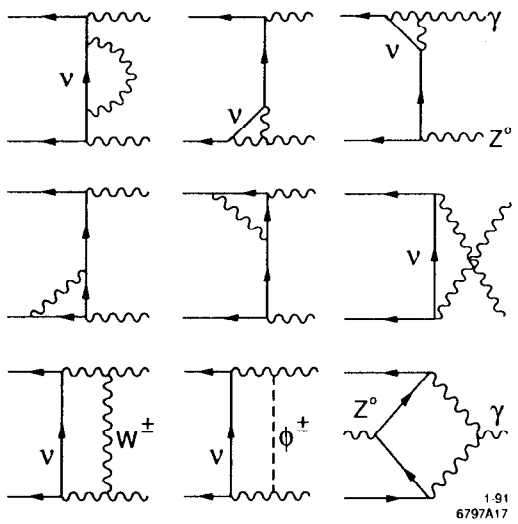

Figure 23. Charged current loop corrections to the production of neutral gauge bosons in e^+e^- annihilation .

The cross section is written,

$$\frac{d\sigma}{d\Omega} = \left(\frac{d\sigma}{d\Omega}\right)_{Tree} \cdot (1 + \delta^{QED} + \delta^{weak}),$$

with the weak correction further broken into contributions from the neutral and charged currents, $\delta^{weak} = \delta^{NC} + \delta^{CC}$. The QED and neutral current corrections that are generated by one loop diagrams are shown in Fig. 22. These are not very interesting. They contain only known vertices, are comparably small, and are symmetric under interchange of any of the particles or helicities. The charged-current corrections, shown in Fig. 23, are more interesting. Diagrams that contain coupling between the Z^0 and W propagators produce the strong energy dependence to δ^{CC} displayed in Fig. 24. The effect of the three-gauge boson coupling is easily isolated by measurements of the energy dependence of the cross section for this

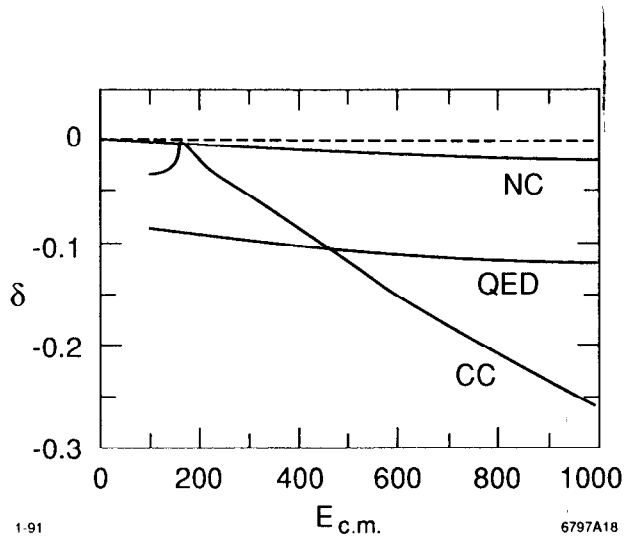

Figure 24. Loop correction to the production of neutral gauge boson pairs by QED, weak neutral currents (NC), and weak charged currents (CC).

process. Perhaps even better, the presence of the left-handed neutrino propagator in the most interesting subset of the diagrams in Fig. 23 projects out these pieces when the initial electron is polarized. A measurement of the left-right asymmetry,

$$A_{LR}(e^+e^- \to \gamma Z^0) \approx -P(e^-) \cdot \delta_\nu^{CC},$$

will allow a direct probe of the couplings between gauge bosons.[1] Notice that a proper evaluation of the correction, δ_ν^{CC} will require knowledge of the strength of these couplings at all momenta! These are not small effects, and can easily be measured with good accuracy.

Strongly Interacting Gauge Bosons

Theories of electroweak symmetry breaking can be divided into those that contain light self-interacting scalar particles, and models which postulate a new level of compositeness of one form or another. These latter theories, technicolor is an example, inevitably lead to strong interactions between gauge bosons. The origins

of these forces, and the particular interaction channels in which they will appear, depend on the details of the model. We start by examining gauge boson interactions in the Standard Model Higgs sector.

The simplest version of the Standard Model contains an SU(2) doublet of complex Higgs fields[23]

$$\phi = \frac{1}{\sqrt{2}}\begin{pmatrix}\phi_1 + i\phi_2 \\ \phi_0 + i\phi_3\end{pmatrix},$$

that are self-interacting. The interaction potential can be written,

$$V_{scalar} = \lambda(|\phi|^2 - <vev>^2)^2$$

and the vacuum expectation value chosen to be,

$$<vev> = \frac{1}{\sqrt{2}}\begin{pmatrix}0 \\ v\end{pmatrix}.$$

The ground state of the Higgs field is then determined by the potential,

$$V_{scalar} = \frac{\lambda}{4}(\phi_1^2 + \phi_2^2 + \phi_3^2 + \phi_0^2 - v^2).$$

With these choices, the Goldstone bosons become

$$\begin{aligned}\omega^{\pm} &= \frac{1}{\sqrt{2}}(\phi_1 \pm i\phi_2) \\ z^0 &= \phi_3 \\ H &= \phi_0 - v,\end{aligned}$$

and the potential can be written,

$$V_{scalar} = \frac{\lambda}{4}(2\omega^+\omega^- + z^0z^0 + H^2 + 2Hv)^2.$$

The mass of the Higgs can be read from this form to be $m_H^2 = 2\lambda v^2$, and for our purposes here, it is best to eliminate λ in favor of m_H,

$$V_{scalar} = \frac{m_H^2}{8v^2}(2\omega^+\omega^- + z^0z^0 + H^2 + 2Hv)^2. \qquad (12)$$

We can determine the value of the vacuum expectation value v from the known masses of the W and Z^0, which are generated by the kinetic energy $(D_\mu\phi)^*(D^\mu\phi)$,

$$m_W = \frac{1}{2}vg.$$

This gives the value,

$$v^2 = \frac{1}{\sqrt{2}G_F} \approx (246\ GeV)^2.$$

From this result and Eq. (12), it is apparent that we can expect the coupling of Goldstone bosons to Higgs scalars to be of order unity when,

$$m_H \sim \sqrt{8}\ (246\ GeV) \approx 700GeV.$$

Let us explore what happens in the region of large m_H. It is useful to first exhibit a connection between the interactions of Goldstone bosons and those of the physically realized W and Z states.

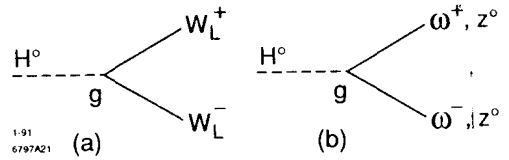

Figure 25. Higgs decays to (a) Longitudinal gauge bosons, and (b) Goldstone bosons.

Consider the decay of the Higgs to massive longitudinal $W_L^{\pm}$ states shown in Fig. 25(a). The matrix element is (c.f. Eq. 9),

$$\begin{aligned}\mathcal{M} &= g m_W \ \epsilon_\mu^L(k) \cdot \epsilon_\mu^L(k) \\ &= g m_W \ (q_0^2 + |\vec{q}|^2)/m_W^2 \\ &= g \left(\frac{m_H^2}{2m_W}\right) \cdot \left(1 + \frac{2m_W^2}{m_H^2}\right) \\ &\approx g \left(\frac{m_H^2}{2m_W}\right).\end{aligned}$$

We have taken the mass of the Higgs to be large compared to the mass of the W-boson in the last line. Now consider the decay of the Higgs to Goldstone bosons shown in Fig. 25(b). We can read the matrix element directly from our expression for the scalar potential,

$$\begin{aligned}\mathcal{M}_{H\omega^+\omega^-} &= 2\mathcal{M}_{Hz^0z^0} = \frac{m_H^2}{v} \\ &= g \left(\frac{m_H^2}{2m_W}\right).\end{aligned}$$

This is an example of the "Equivalence Theorem" — to accuracy m_W^2/s, the interactions of longitudinal gauge boson states are given by the interactions of the Goldstone bosons that create them.

Gauge Boson Scattering

As an example of the phenomenology of a strongly-interacting Higgs sector, consider the reaction,

$$W^+W^+ \ \rightarrow \ W^+W^+.$$

The Feynman diagrams that contribute to this reaction are shown in Fig. 26. The Higgs contribution to the amplitude is not small since the W mass is large. The leading dependencies on center-of-mass energy scale as s^2/m_W^4 and s/m_W^2, but cancel in the sum of the three diagrams. What is left are terms proportional to s, that are well-behaved for large Higgs masses, and others proportional to $(m_H/m_W)^2$ that are not.

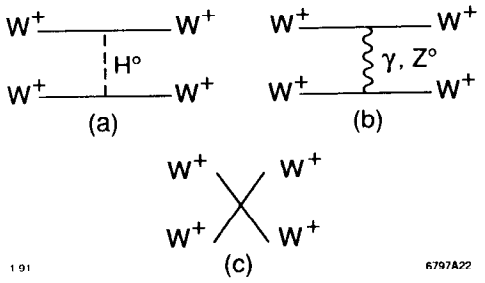

Figure 26. Feynman diagrams that contribute to W^+W^+ scattering.

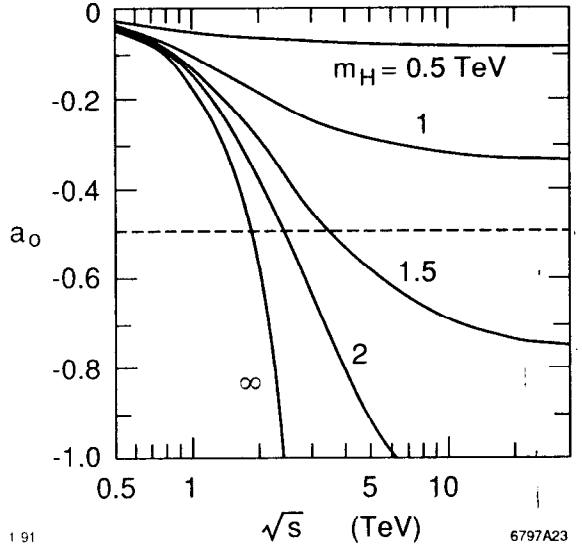

Figure 27. S-wave amplitude for W^+W^+ scattering calculated with the Equivalence Theorem for values of the Standard Model Higgs mass.

As expected, the problems arise in the scattering of longitudinally polarized bosons by Higgs exchange. We can use the Equivalence Theorem to write the amplitude for Higgs exchange in the limit s and $m_H^2 >> m_W^2$,

$$i\mathcal{M} = \frac{m_H^2}{v}\left(\frac{t}{t-m_H^2} + \frac{u}{u-m_H^2}\right).$$

Individual partial waves in the scattering amplitude will violate unitarity if m_H becomes too large. To see where this occurs, expand the amplitude,

$$i\mathcal{M} = -16\pi \sum_J (2J+1)a_J(s)P_J(cos\theta).$$

The s-wave dominates, and we can calculate[24],

$$\begin{aligned} a_0(s) &= \frac{q_W}{32\pi\sqrt{s}}\int_{-1}^{1}(-i\mathcal{M})\ dcos\theta \\ &= -\frac{1}{16\pi}\left(\frac{m_H}{246}\right)^2\left[1-\frac{m_H^2}{s}ln\left(1+\frac{s}{m_H^2}\right)\right]. \end{aligned}$$

The resulting partial wave amplitude is shown in Fig. 27 as a function of center-of-mass energy for several values of the mass of the Higgs. Partial wave unitarity requires,

$$|a_0|^2 \leq |Im(a_0)|,$$

or, $|Re(a_0)| \leq \frac{1}{2}$. Apparently, for Higgs masses greater than about 1.2 TeV, perturbation theory fails at large center-of-mass energies! The gauge boson sector becomes strongly interacting — something else must begin to occur if there is no "light" Higgs particle.

The manifestation of new physics in gauge boson interactions may be dramatic, as the appearance of new resonances would be, or may be substantially more subtle. Fig. 28 shows the cross sections predicted by the Standard Model perturbative

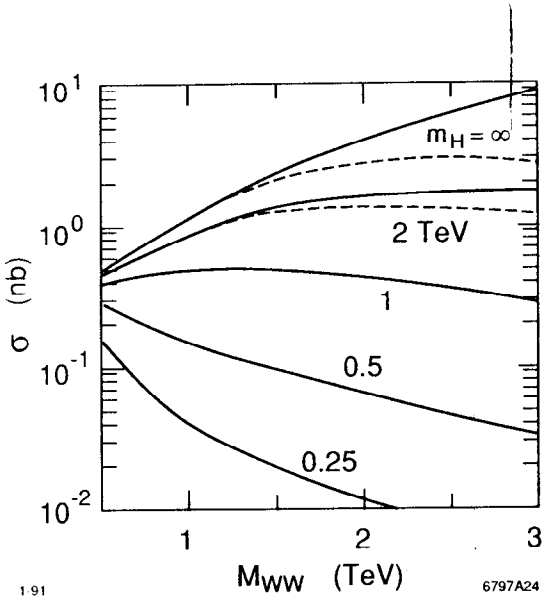

Figure 28. Cross section for W^+W^+ scattering in the Standard Model for a number of Higgs masses. The dashed curves are cross sections calculated with the constraint that the partial wave amplitude never exceeds the limit imposed by unitarity.

amplitude for a variety of Higgs masses. The maximum cross section allowed by partial wave unitarity is also shown for very massive Higgs particles. The cross section at large center-of-mass energy is small in the presence of light Higgs particles since the gauge cancellations are then complete, but in the absence of these scalars, the cross section is ill-defined in the Standard Model. Fig. 29 compares a number of models and *ad hoc* calculations of the W^+W^+ scattering cross section at TeV center-of-mass scales. The differences between the various possibilities are typically factors of two to four.

It is, of course, possible to consider the process,

$$W^+W^- \rightarrow W^+W^-,$$

shown in Fig. 30. This is the well-recognized Higgs discovery reaction that will

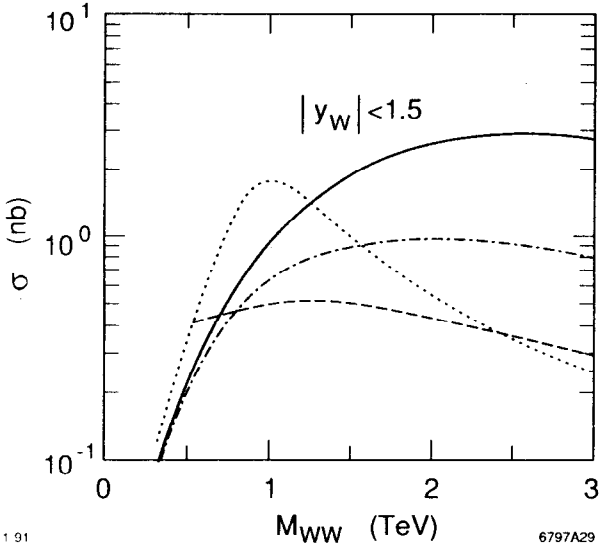

Figure 29. Various models for the W^+W^+ cross section. The solid curve is the unitarized Standard Model with infinite Higgs mass, the dashed curve is the Standard Model with $m_H = 1$ TeV. The dotted curve is chiral model of Einhorn[25], and the dot-dashed curve is a result obtained[24] by rescaling low energy $\pi^+\pi^+$ scattering.

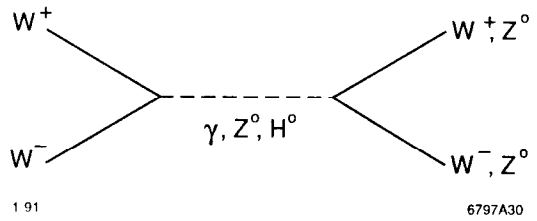

Figure 30. Production of W^+W^- in e^+e^- annihilation .

proceed through s-channel γ, , Z^0, and Higgs propagators. There are still the t and u-channel graphs and four-boson contact terms that will behave as in the like-sign W-boson case. If a light Higgs exist, then it will appear as a resonance in this channel, and gauge invariance will guarantee that the cross section is well-behaved. But in its absence, this process is plagued by all of the difficulties that we have discussed in this section.

Experimental Studies of WW Scattering

To exhaust the possible avenues to new physics, and fully explore any that is found, it is essential to study gauge boson scattering in several channels,

$$I = J = 0 \quad (C = +)$$
$$I = J = 1 \quad (C = -).$$

The C-odd p-wave is strongly excited in e^+e^- annihilation , and new physics will appear as a violation of the Standard Model prediction for the production of longitudinal W_L pairs. A particular example is shown in Fig. 31. Final state rescattering of the boson pair occurs through the exchange of a techni-rho meson.

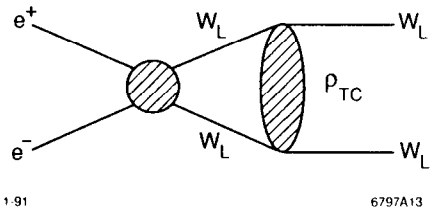

Figure 31. Final state interaction of W-pairs produced in e^+e^- annihilation .

In technicolor theories[26], matter fields are techniquarks and technileptons, which are bound by strong interactions generated by an underlying non-Abelian technicolor gauge group. Techniscalars (the "pions" of technicolor) play the roles of the Higgs and the longitudinal boson states. There are additionally, vector states, for example the techni-rho ρ_{TC}. The mass of the techni-rho is unspecified by the

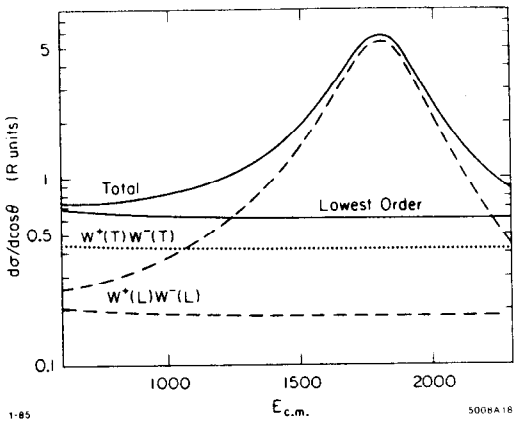

Figure 32. Production of a technirho resonance in the longitudinal W-pair channel of e^+e^- annihilation .

theory, but a guess is often made by analogy with lower energy hadron spectroscopy,

$$m_{\rho_{TC}} \sim m_\rho \left[\frac{< vev >_{Higgs}}{f_\pi}\right],$$

where the pion decay constant $f_\pi \approx 90$ MeV. This yields a value of $m_{\rho_{TC}} \sim 1.8$ TeV. The width of the techni-rho can similarly be scaled from that of the ordinary rho-meson to find a value of order 0.3 TeV. The resulting cross section, shown in Fig. 32, is dramatically different from the Standard Model prediction even at fairly low center-of-mass energies. Efforts are underway[27] to parameterize in more detail the phenomology of the W-pair final state produced by e^+e^- annihilation in a range of models such as those shown in Fig.29.

WW Fusion

While there is no way to experimentally produce beams of W-bosons, it is possible to realize WW scattering in the C-even channel through the peripheral process shown in Fig. 33. The reaction rate is characterized by a splitting function,

$$f_{V/l,q} = f_{V/l,q}(Q^2, x),$$

which gives the effective boson flux for beams of leptons or quarks. The Weizsacker-Williams photon flux often associated with a beam of high-energy electrons is a particular example of this. In fact, calculations have been made[28] using an analogous "Equivalent W Approximation". At $s >> m_W^2$, and to $\sim 20\%$ accuracy,

$$f_{W_T} = \frac{\alpha_W}{8\pi} \frac{[1+(1-x)^2]}{x} \ln\left(\frac{Q^2}{m_W^2}\right)$$
$$f_{W_L} = \frac{\alpha_W}{4\pi} \frac{(1-x)}{x}.$$

The equivalent flux of massive bosons has essentially the same form as the equivalent photon flux, and as shown in Fig. 34(a), the flux of longitudinal bosons is about two orders of magnitude smaller. The effective boson-boson luminosity is shown in Fig. 34(b) for a very high energy electron-positron collider, and in Fig. 35 for the SSC. It is clear that studies of longitudinal boson scattering must be done against a considerably larger background of W_TW_T and W_TW_L events.

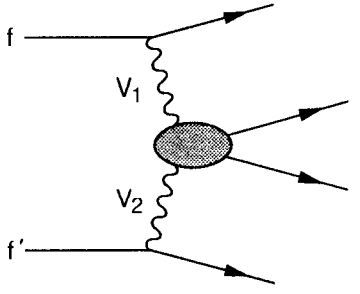

Figure 33. Peripheral scattering of gauge bosons in e^+e^- collisions.

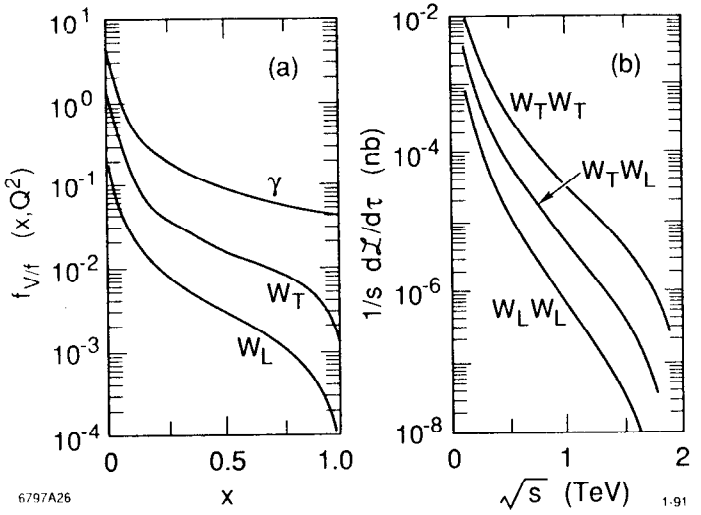

Figure 34. (a) The effective flux of gauge bosons created by a high energy electron beam. (b) The brightness of WW collisions at a 2 TeV e^+e^-collider.

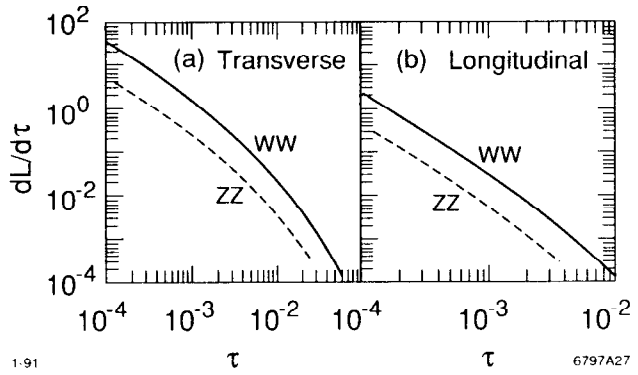

Figure 35. The luminosity of W_TW_T and W_LW_L collisions at the SSC.

As a specific case, we consider the production of W^+W^- pairs at the SSC. These oppositely-charged pairs will be produced both by boson-fusion and by $q\bar{q}$ annihilation. The expected[29] differential cross section (including the resonant piece for several Higgs masses) is shown in Fig. 36. The W-pair is detected only when one of the bosons decays to an electron or a muon. There are large backgrounds to this process from associated production of W's and quark jets by quark and gluon interactions, and from the production and decay of heavy top quarks. A Monte Carlo study has been done[30] at the "four-vector" level. Events were generated without inclusion of the imperfections inherent in any detector (the detector was also assumed to perfectly hermetic), and events were selected with the following criteria,

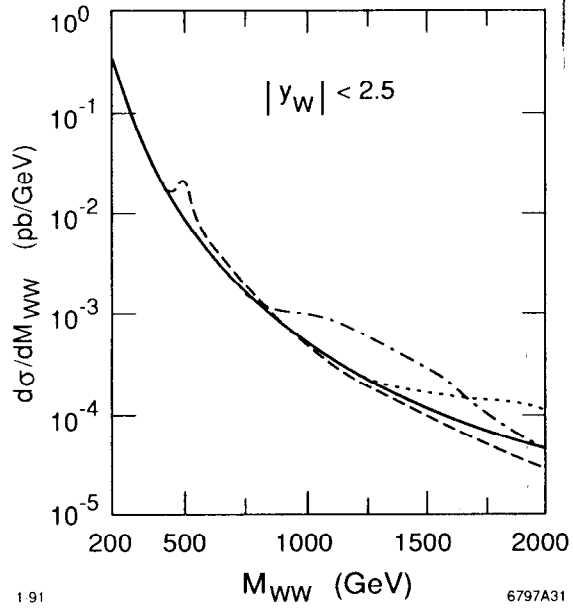

Figure 36. The WW differential cross section at the SSC. The curves include production through $q\bar{q}$ annihilation as well as the W-fusion process with Higgs of 0.5 Tev, 1.0 TeV, and 1.5 TeV mass.

(*i*) The topology of the event was correct.

(*ii*) Two jets were found with invariant mass within 5 GeV of the known W mass.

(*iii*) The total number of charged particles in the pair of jets taken as the W candidate was less than 20.

The number of signal and background events that survive these cuts (normalized to one year of running at the SSC luminosity of $10^{33}\text{cm}^{-2}\text{s}^{-1}$) is tabulated:

M_{WW} (GeV)	$q\bar{q}$	Higgs (m_H = 1TeV)	Low ($m_H = \infty$)	O(2N)	Wjj
850-950	39	57	5	9	136
950-1050	33	66	6	8	91
1050-1150	27	54	6	6	58
1150-1250	20	34	5	5	58
1250-1350	16	19	5	4	32

Boson pairs produced by $q\bar{q}$ annihilation, and misidentified Wjj events are backgrounds to the possible signal from the boson-boson scattering process. The "Low" and "O(2N)" models are those shown in Fig. 29 as representative of possible alternatives to the Standard Model. It is clear that it will be extremely difficult to extract any signal if the channel is not resonant, and even more difficult to discriminate between the various models of the underlying theory.

The boson-fusion process is more easily isolated in electron-positron collisions, but the machine luminosity required to reach large WW center-of-mass energies is quite large. The reaction, shown in Fig. 37, results in two neutrinos that carry away significant energy in the final state. The observed WW system is produced with momentum transverse to the e^+e^- beamline,

$$p_t(WW) \sim m_W,$$

which appears as missing p_t in the event.

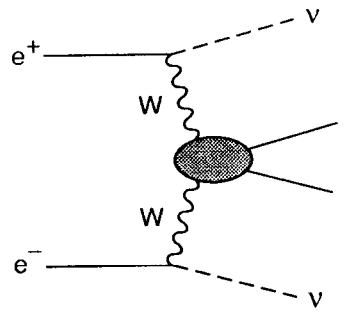

Figure 37. The W-fusion reaction in e^+e^- collisions.

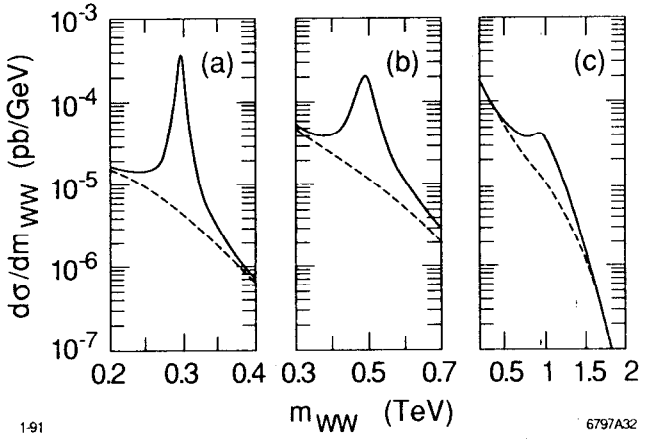

Figure 38. Cross sections for W-fusion in e^+e^- collisions at (a) $\sqrt{s}$ = 0.5 TeV with a 300 GeV Higgs, (b) $\sqrt{s}$ = 1.0 TeV with a 500 GeV Higgs, and (c) $\sqrt{s}$ = 2.0 TeV with a 1.0 TeV Higgs. The dashed curves are the predictions of the Standard Model with m_H taken to infinity.

The expected cross sections are shown in Fig. 38 at three machine energies. The presence of a Higgs resonance can be detected, and it decay properties studied[31]

if its mass is less than $\approx$ 75% of the e^+e^- center-of-mass energy, but to generate a sufficient numbers of non-resonant WW scattering events at masses above 1 TeV to fully resolve the physics in these reactions, will require machines with e^+e^- center-of-mass energies of 2 TeV or greater, and luminosities nearing $10^{34}cm^{-2}s^{-1}$. For example, at 2 TeV the differential cross section, shown in Fig. 38, corresponds to 10 produced events per 100 GeV bin at m_{WW}= 1 TeV in a data exposure of 10 fb^{-1}.

It is clear that in the absence of striking features in gauge boson interactions, such as the presence of Higgs scalars or technicolor particles, it is going to require some time and considerable effort at future colliders to dig out the contents of what has become called "Physics at the TeV Scale".

Acknowledgement

The author is pleased to thank T.Barklow and M.Peskin for sharing their work, interest, and excitment with the physics discussed in these lectures, and E.Yehudai for many discussions and insights to his work.

REFERENCES

1. F. Dydak, Proceedings of the 25th International Conference on High Energy Physics, Singapore, 1990.
2. See, for example, "Gauge Theories of the Strong, Weak, and Electromagnetic Interactions", by C. Quigg, Benjamin/Cummings, Menlo Park, CA, USA, 1983.
3. CERN 86-02, ed. J.Ellis and R.Peccei, 1986.
4. O. P. Sushkov, V. V. Flambaum, and I. B. Khriplovich, Sov. J. Nucl. Phys. 20, 537, 1975; W. Alles, Ch. Boyer, and A. Buras, Nucl. Phys. B119, 125, 1977.
5. K.Hagiwara, R.D.Peccei, D.Zeppenfeld, and K.Hikasa, Nucl. Phys. B282, 253, 1987.
6. G.L.Kane, J.Vidal, and C.P.Yuan, Phys.Rev. D39, 2617, 1989.
7. K.B.Samuel, M.A.Samuel, and G.Li, OSU Research Note 218, 1989.
8. U.Baur and E.L. Berger, CERN-TH.5517/89 and ANL-HEP-PR-89-86, 1990.
9. T.Himel and J.Siegrist, SLAC-PUB-3572, 1985; R.Blankenbecler and S.D.Drell, Phys.Rev. D37, 1988; see also, P.Chen, "Review of Linear Collider Beam-Beam Interaction", contributed to the U.S. Particle Accelerator School, Batavia, Illinois, 1987, and references therein.
10. G. S. Abrams, *et al.*, Phys. Rev. Lett. 63, 2447, 1989.
11. Proceedings of the Workshop on Physics at Future Accelerators, La Thuile, 1987, J. H. Mulvey, ed., CERN 87-07, 1987; C.Ahn, et al., "Opportunities and Requirements for Experimentation at a Very High Energy e^+e^- Collider", SLAC-Report-329, 1988; Proceedings of the Summer Study on High Energy Physics in the 1990's, Snowmass, 1988, S. Jensen, ed., World Scientific, Singapore, 1989.
12. T.Barklow and C.Simopolous, private communication.

13. E.Yehudai, SLAC-PUB-5008, 1989, (Ph.D. Thesis).

14. G.L.Kane, J.Vidal, and C.P.Yuan, Phys.Rev. D39, 2617, 1989.

15. L.F.Abbott and E.Farhi, Phys.Lett. 101B, 69, 1981; Nucl.Phys. B189, 547, 1981.

16. S.J.Brodsky, A.J.Davies, and R.R.Volkas, Phys.Rev. D39, 2797, 1989.

17. K.F. Smith et al., Phys.Lett. B234, 191, 1990.

18. S.Weinberg, Phys.Rev.Lett 63, 2333, 1989.

19. Xiao-Gang He and B.H.J.McKellar, UM-P-90/39(Melbourne),1990.

20. M.Pundurs, ANL-HEP-PR-89-127, 1989.

21. F.M.Renard, Nucl.Phys. B196, 93, 1982.

22. M.Bohm and Th.Sack, Z.Phys. C35, 119, 1987.

23. The Higgs is discussed extensively in the literature. See for example, J.Gunion, H.Haber, G.Kane, and S.Dawson, "The Higgs Hunter's Guide", UCD-89-4, 1989, and references therein.

24. V.Barger, K.Cheung, T.Han, and R.J.N.Phillips, MAD/PH/556, 1990.

25. M.B.Einhorn, Nucl.Phys. B246, 75, 1984.

26. E.Fahri and L.Susskind, Phys. Repts. 74, 277, 1981.

27. M.Peskin, private communication.

28. S.Dawson, Nucl.Phys. B249, 42, 1985.

29. M.Duncan, G.L.Kane, and W.Repko, Nucl.Phys. B272, 517, 1986.

30. G.L.Kane and C.-P.Yuan, Phys. Rev. D40, 2231, 1989.

31. See, for example, M.Levi, "W^+W^- Interactions and the Search for the Higgs Boson", Proceedings of the 17th SLAC Summer Institute, 187, 1989, and references therein.